IEEE Photonics Journal
An IEEE Photonics Society Publication

Open Access

Automatic Modal Wavefront Estimation and Correction for Optical Aberration

Volume 11, Number 1, February 2019

Xiaomin Lai
Chen Xu
Yafeng Liu
Kaihua Wei
Kaihua Wu

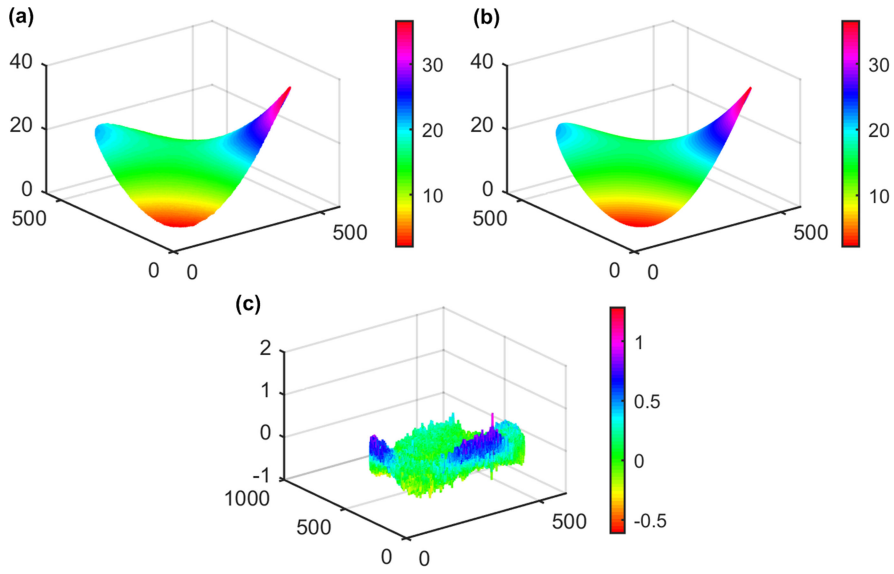

DOI: 10.1109/JPHOT.2018.2888549
1943-0655 © 2017 IEEE

IEEE photonics SOCIETY

IEEE

Automatic Modal Wavefront Estimation and Correction for Optical Aberration

Xiaomin Lai,[1] **Chen Xu**,[1] **Yafeng Liu**,[2] **Kaihua Wei**,[1] **and Kaihua Wu**[1]

[1]College of Life Information Science and Instrument Engineering, Hangzhou Dianzi University, Hangzhou 310000, China
[2]College of Life Science and Technology, Huazhong University of Science and Technology, Wuhan 430074, China

DOI:10.1109/JPHOT.2018.2888549

Manuscript received November 20, 2018; accepted December 14, 2018. Date of publication December 18, 2018; date of current version January 8, 2019. This work was supported by the National Natural Science Foundation of China under Grant 61605039, under Grant 11304070, and under Grant 61372155).
Corresponding author: Kaihua Wei and Kaihua Wu (e-mail: weikaihua@hdu.edu.cn; wukaihua@hdu.edu.cn).

Abstract: Modal estimation of aberration can quantify the amount of aberration, which plays an important role in optical system optimization, aberration correction, and so on. Here, we propose a simple but effective method to find the modal wavefront of aberration. Once the aberrated wavefront has been detected, it will be automatically analyzed with a method based on one-dimensional standard polynomial fitting. According to the analysis, the modal wavefront and the property of aberration can be obtained for further studies. Here, for example, we show that it can be used to calculate the optimal correction wavefront. Experiments were implemented to testify the correctness and effectiveness of this method. This method provides users another option for aberration interpretation.

Index Terms: Adaptive optics, aberration, holography, spatial light modulators.

1. Introduction

Aberration correction and interpretation are critical issues in optical imaging system. Aberration interpretation (also known as aberration decompositon) plays an important role in optical system design and optimization, because it can decompose the aberration into normal models and quantify the amount of aberration. It is also the crucial step for aberration correction.

Aberration is a common problem in optical systems. [1] Although it can be minimized via careful alignment and high-quality instruments, aberration still occurs because it is very sensitive to defects, such as the inherent optical imperfection of biological samples. It is of fundamental interest whether aberration can be corrected in a simple but effective way. In principle, once aberration has been measured, it can be corrected by presetting a wavefront that is optically conjugated. [2], [3] To measure aberrations, there are all kinds of wavefront sensors based on, for example, interferometry [4], [5], analyzing optical patterns [6], Hartmann-Shack wavefront sensor [7], and so on [8], [9]. To preset the correction wavefront, one can use an off-the-shelf correctors, such as a spatial light modulator (SLM) [10]–[12] or a deformable mirror [13]–[16]. Nowadays, both steps have been well developed and can be easily accomplished. The crucial but less noticed problem is how to get the correction wavefront from the measured signals, i.e., the mystery of the "black box" that magically translate the signals from the wavefront sensor to the signals for correctors [17]. This is a

fundamental issue behind the adaptive optics system [17]. To determine the appropriate parameters for corrector, first the sensor signals should be properly analyzed, such as sorting out the meaning of signals and finding a modal representation of aberration.

Many efforts have been devoted to find the modal estimation of the aberration signals obtained with a Hartmann-Shack wavefront sensor (or a shearing interferometers), because this type of sensor measures the local slopes (or difference) rather than the original wavefront [17]–[19]. However, for wavefront sensors based on digital holography, the modal estimation is much simpler since it directly detects the wavefront under test itself. Usually, people use the two-dimensional (2D) Zernike polynomial fitting (ZPF) to decompose the detected wavefront [18], [20]. Then, they can use the decomposed coefficients to calculate the correction wavefront. Thus, with the modal wavefront estimation aberrations can be represented by modal series, such as the Zernike polynomials or power series [17], with which the phase can be found at any points instead of a few pixel points on sensor.

There is one type of method, some image-based zonal correction methods, in which the modal estimation procedure can be avoided when determining the correction wavefront, because the correction wavefront is determined during the aberration measuring process [1], [21]–[27]. These methods typically introduce certain metrics to evaluate the correction quality. The correction phase is the one that minimize or maximize such metrics. These methods are especially suitable for applications where the incident light cannot be effectively reflected or transmitted. However, the measuring process is time consuming [27], or complicated. On the other hand, in these methods, when people want to know the amounts of aberrations, they still have to analyze the aberration using modal representation, such as the 2D ZPF. Thus, there is a wide need of modal wavefront estimation because it not only acts as a crucial step for aberration correction but also gives a quantified description on aberrations.

Here, we propose a simple but powerful method to automatically estimate the modal representation of aberration after it being measured with a classical digital holographic wavefront sensor. The wavefront is automatically analyzed using a method based on one-dimensional (1D) polynomial fitting instead of 2D ZPF. With this method, the components of aberration and their amounts can be acquired. To test the correctness, the modal estimation was used to predict the correction wavefront. Experimental results show that aberrations have been effectively compensated, proving the correctness of modelling.

2. Theoretical Model

The wavefront was measured with a digital holographic wavefront sensor. We denote the measured wavefront as φ. Here, instead of using Zernike polynomials, we represent the wavefront with a power series in Cartesian coordinates. For higher accuracy, usually a few iterations are needed to find the right modal description. For each iteration, 1D standard polynomial fittings of order n are implemented on two profiles along the x_0 and y_0 (vertical to x_0) axes. The axis x_0 corresponds to the direction whose standard deviation (STD) is maximum.

The fitting results along the two profiles are:

$$f_i(x_0) = [a_{0i},\ a_{1i},\ a_{2i},\ \ldots\ a_{ni}]\, X_0^T,$$
$$f_i(y_0) = [b_{0i},\ b_{1i},\ b_{2i},\ \ldots\ b_{ni}]\, Y_0^T, \tag{1}$$

respectively. In Eq. (1), the a_{ni} and b_{ni} ($n = 0, 1, 2, 3\ldots$) are polynomial coefficients, X_0 and Y_0 are vectors described as $X_0 = [x_0{}^0, x_0{}^1, x_0{}^2 \ldots\ x_0{}^n]$ and $Y_0 = [y_0{}^0, y_0{}^1, y_0{}^2 \ldots\ y_0{}^n]$, respectively, $[\cdot]^T$ stands for a transposition, and i is the times of iteration. Using the results in Eq. (1), the 2D aberration representation in coordinate x_0y_0 can be obtained by $f_i(x_0) + f_i(y_0)$.

According to coordinate transform, the relationship between axes x_0y_0 and the principle axes xy is:

$$\begin{bmatrix} x_0 \\ y_0 \end{bmatrix} = \begin{bmatrix} \cos\theta_i & \sin\theta_i \\ -\sin\theta_i & \cos\theta_i \end{bmatrix} \begin{bmatrix} x \\ y \end{bmatrix} \tag{2}$$

where θ_i is the angle between x_0 and x at iteration i.

The decomposed 2D wavefront can be described using a power series as:

$$\varphi_{xyi}(x, y) = \sum_{l=0}^{L} \sum_{k=0}^{K} P_{k,l,i} x^k y^l \tag{3}$$

where K and L are the highest order of polynomials x and y, respectively. The coefficient $P_{k,l,i}$ in Eq. (3) can be derived using Eq. (1) and Eq. (2) as:

$$P_{k,l,i} = C(k+l, l)\left[a_{(k+l)i}\cos^k\theta_i \sin^l\theta_i + b_{(k+l)i}(-\sin\theta_i)^k \cos^l\theta_i\right]. \tag{4}$$

where $C(k + l, l)$ stands for the number of l-combinations from a given set that has $k + l$ elements.

When the amount of aberration is large, it cannot be fully quantified within one fitting. Therefore, as we mentioned before a few iterations are needed. Usually, the most dominant aberrations will be find in the first iteration and be removed as $\varphi_{re} = \varphi - \varphi_{xyi}$. By doing this, these less dominant aberrations became more obvious. The remaining phase φ_{re} will be fitted again and the procedure will be repeated until the STD of φ_{re} is small enough, i.e., smaller than a threshold value. When the STD of remaining phase is very small, the phase distribution is nearly flat except for some fluctuations of noise. That means total aberrations have been fully quantified.

Then, the modal estimation can be obtained by summing up all φ_{xyi} from every iteration. After M iterations, the modal estimation of measured wavefront is:

$$\varphi_{xy}(x, y) = \sum_{l=0}^{L} \sum_{k=0}^{K} P_{k,l} x^k y^l. \tag{5}$$

where the final coefficients $P_{k,l}$ of $x^k y^l$ is:

$$P_{k,l} = \sum_{i=1}^{M} C(k+l, l)\left[a_{(k+l)i}\cos^k\theta_i \sin^l\theta_i + b_{(k+l)i}(-\sin\theta_i)^k \cos^l\theta_i\right] \tag{6}$$

which is the sum of $P_{k,l,i}$ from every iteration. In Eq. (6), we can see that using the 1D standard polynomial fitting coefficients a_{ni} and b_{ni}, the aberration coefficients $P_{k,l}$ can be calculated. The final residual phase is $\varphi_{re} = \varphi - \varphi_{xy}$. The final residual phase will not be fitted anymore as its STD is very small which means it is nearly flat.

The modal estimation given in Eq. (6) and Eq. (5) provides a mathematical expression of aberration. It is a continuous wavefront representation with which the phase at various locations can be obtained. Moreover, according to Eq. (6) and Eq. (5), the amount of each aberration can be calculated, which is important for the analysis of aberrations property. For example, if P_{21} is zero, it means there is no aberration x^2y existed in this system. Meanwhile, the aberration coefficients can be related to that of the classical optical aberration modes. [17], [28] They can also be transformed to the coefficients of Zernike polynomials if it is necessary, for example, when the orthogonality of Zernike polynomial is preferred.

It should be noted that, as the fitting is implemented along the direction with the largest aberration, the iteration converges quickly. Moreover, the aberration is decomposed without the need of 2D Zernike polynomials. Comparing with the 2D ZPF, 1D polynomial fitting is more flexible, users friendly, easier to implement and does not have strict request on pupil shape.

The correction wavefront can be calculated according to the modal representation in Eq. (5). Set $x_s y_s$ as the coordinates of corrector. The angle between coordinates $x_s y_s$ and xy is β and the centre of $x_s y_s$ is shifted (Δx, Δy) from that of xy. Using the coefficients $P_{k,l}$ given in Eq. (6), the correction wavefront can be calculated as

$$\varphi_{SLM}(x_s, y_s) = -\sum_{l=0}^{L} \sum_{k=0}^{K} P_{k,l}\left(x'_s\right)^k \left(y'_s\right)^l \tag{7}$$

where $x_s' = (x_s - \Delta x)\cos\beta - (y_s - \Delta y)\sin\beta$ and $y_s' = (x_s - \Delta x)\sin\beta + (y_s - \Delta y)\cos\beta$. The signal on each pixel of corrector can be calculated using Eq. (7). If the modal estimation is right, which

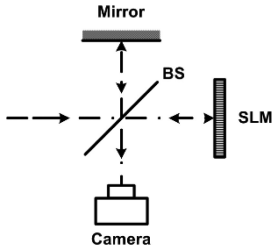

Fig. 1. Simplified schematic of optical system. The wave was divided into two waves. One of them was reflected by SLM while the other one was reflected by a mirror. A camera was used to record the interference patterns.

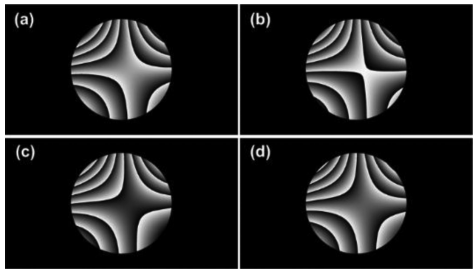

Fig. 2. Phase aberrations (φ_o) addressed to SLM. The aberrations for (a–d) are the same but with four different initial phases: $\pi/2$, π, $3\pi/2$, 2π, respectively. Color bar: from black to white the phase is 0 to 2π.

means the coefficients in Eq. (6) are correct, aberrations can be compensated with the wavefront in Eq. (7).

For simplicity we assume that the directions and centres of $x_s y_s$ and xy are the same but their sampling intervals are different. This is the case usually encountered in practice. Then, the correction wavefront is simplified to

$$\varphi_{SLM}(x_s, y_s) = -\sum_{l=0}^{L}\sum_{k=0}^{K} P_{k,l} x_s^k y_s^l. \tag{8}$$

The wavefront in Eq. (8) will be used to compensate the aberration and confirm the correctness of modal estimation.

3. Experiments

Experiments were implemented to verify the effectiveness of the proposed method. First the aberration was measured with a sensor based on the Michelson interferometer. A liquid crystal SLM (Holoeye, Pluto VIS) was used as the corrector, which displayed the correction wavefront. The essential components of optical system are given in Fig. 1. A beam splitter (BS) divided a collimated and expanded laser beam into two waves. The wave reflected by SLM (O) interfered with the reference wave (R) reflected by a mirror. Two waves were on-axis. The interference patterns were recorded with a complementary metal oxide semiconductor (CMOS) camera (Thorlabs, DCC3260 M). As the active area of the SLM is larger than that of the camera, a relay system (not given in Fig. 1) of ratio 1/2 was placed between the SLM and the camera.

To produce a dramatic aberration, here the SLM was also used to introduce a large amount of aberration. Thus, the total aberrations in the system include the intentionally introduced aberration φ_o and aberrations caused by other defects of our system. We used four-step phase shifting [29] to decode the phase distribution of OR^*. That means the aberration φ_o was addressed to SLM four times with four different initial phases, as given in Fig. 2. It can be seen that there were obvious astigmatism and coma aberrations in φ_o.

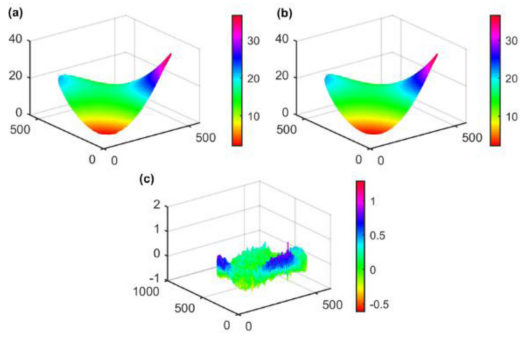

Fig. 3. Comparison between the measured wavefront and the modal wavefront. (a) Measured wavefront, (b) modal wavefront after three iterations, (c) residual phase distribution. The STDs for (a–c) are 5.46, 5.42, and 0.17, respectively. Only regions of interest (ROI) are shown. The color bars indicate the phase in radians.

TABLE 1

Coefficients of the Modal Wavefront Expressed in Scientific Notation (p Times Ten Raised to the Power of q)

	P_{00}	P_{10}	P_{01}	P_{20}	P_{02}	P_{11}	P_{30}	P_{03}	P_{12}	P_{21}	P_{40}	P_{04}	P_{22}	P_{31}	P_{13}
Mantissa p	1.7	5.6	-1.4	-2.2	6.5	-2.7	2.7	3.0	3.0	-2.5	1.2	-9.5	1.4	6.1	8.5
Exponent q	01	-04	-03	-07	-08	-06	-11	-11	-10	-11	-14	-15	-14	-15	-15

With every phase distribution in Fig. 2, one hologram was recorded. Then, the phase distribution of OR^* was decoded from holograms. We should point out that, as the reference wave R was an on-axis plane wave that can be described by a constant, the decoded phase distribution of OR^* was the total phase aberration of optical system. After this, the measured aberration was unwrapped with a standard 2D phase-unwrapping algorithm [30].

3.1 Modal Wavefront Estimation

The measured aberration after phase unwrapping is showed in Fig. 3(a) presented in three-dimensional (3D) perspective. If there was no aberration, the phase distribution should be flat. However, from Fig. 3(a), it can be seen that the surface was in a sophisticated shape indicating there were large amount of aberrations.

The proposed method was used to find the modal representation of aberrations in Fig. 3(a). Here, we limited the polynomial order of fitting to $n = 4$ as it already contains most part of the aberrations encountered in optical system. The threshold of the STD of residual phase was set to 0.5, and the fitting process terminated after three iterations. Fig. 3(b) gives the modal wavefront obtained with Eq.(5). Fig. 3(c) gives the final residual phase distribution obtained by subtracting Fig. 3(b) from Fig. 3(a). The STDs of the phase distribution for Fig. 3(a–c) are 5.46, 5.42 and 0.17, respectively. One can also adopt more iteration for smaller residual phase when it is necessary, as long as the signal to noise ratio of aberration is high enough.

First, from Fig. 3(a) and Fig. 3(b), we can see that the modal wavefront agrees well with the measured wavefront, and their STDs are close (5.46 vs. 5.42). Second, as Fig. 3(c) shows the difference between Fig. 3(a) and Fig. 3(b), the STD of Fig. 3(c) is small, which also indicates the difference between the measured wavefront and the modal wavefront is small.

The coefficients of modal wavefront (obtained with Eq. (6)) are given in Table 1, expressed in scientific notation, as $p*10^q$ where p is mantissa and q is exponent. The results can be used to analyse the property of aberration. From the coefficients in Table 1, it can be seen that there were many kinds of aberrations existed in this system. Besides of P_{00}, the most significant aberration

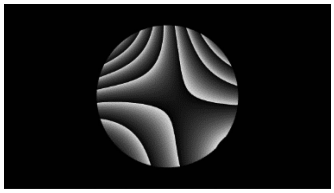

Fig. 4. Correction wavefront obtained with the coefficients of modal wavefront given in Table 1. Color bar: from black to white the phase is 0 to 2π.

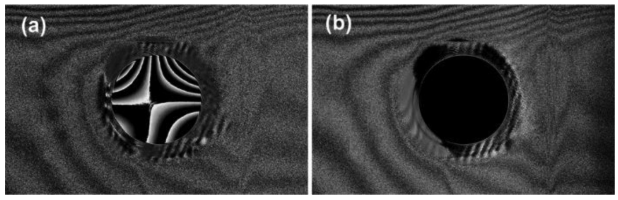

Fig. 5. Phase distribution before (a) and after (b) correction. The STDs in the ROI (inside the circles) of (a) and (b) are 5.46 and 0.24 respectively. Color bar: from black to white the phase is $-\pi$ to π.

is the one with coefficients P_{10} and P_{01} indicating that the most significant aberration is tilt. The secondary aberration is the one with coefficients P_{11}, P_{20}, and P_{02}, which mainly result from astigmatism aberration. Moreover, there are also obvious coma aberrations as coefficients P_{12} and P_{21} are also noticeable. The astigmatism and coma aberration can also be observed from the intentionally introduced aberration in Fig. 2, indicating the possibility that the aberrations have been correctly represented. Meanwhile, there are also little arrow aberration according to P_{30} and P_{03}. The other aberrations are negligible as their coefficients are very small.

It should be noted that, here the coefficients of intentionally introduced aberration (given in Fig. 2) are not given for comparison. That is because, although most of the measured aberration is the intentionally introduced aberration, it also includes other aberrations caused by the imperfection of optical system, for example the flatness deviation of SLM [25], [31], [32]. Thus, it is meaningless to directly compare them. Therefore, we used other methods to exam the correctness of the modal wavefront.

3.2 Aberration Correction

The coefficients given in Table 1 were used to calculate the correction wavefront according to Eq. (8) as we have ensured that the directions and centres of CMOS and SLM are the same. Fig. 4 presents the obtained correction wavefront. If aberration has been represented correctly, it can be expected that using the wavefront given in Fig. 4, the aberration will be corrected.

In Fig. 4, from the profile along the $+45$ degree direction, we can see that for each period of wrapped phase, the phase changes from white to black with increasing of radius. Meanwhile, for the aberration given in Fig. 2, the corresponding phase changes from black to white. That means their trends of changing are opposite. Similar phenomenon can be observed in other directions. It implies the possibility that the correction wave front can offset the aberration.

Both the intentionally introduced aberration (given in Fig. 2) and the correction wavefront (given in Fig. 4) were addressed to SLM, as $\varphi_o + \varphi_{SLM}$ where φ_o is the pre-introduced aberration and φ_{SLM} is the correction wavefront. The measured phase distribution after correction is given in Fig. 5(b). Fig. 5(a) corresponds to the measured aberration before correction displayed in wrapped status. The unwrapped phase of the region of interest (ROI) in Fig. 5(a) has been shown in Fig. 3(a).

The efficiency of correction can be evaluated by measuring the STD of the phase distribution over ROI. The STD of the ROI in Fig. 5(b) was 0.24, while that of Fig. 5(a) was 5.46 (calculated from the unwrapped data). Unlike Fig. 5(a), there was no observable aberration in Fig. 5(b) and its STD

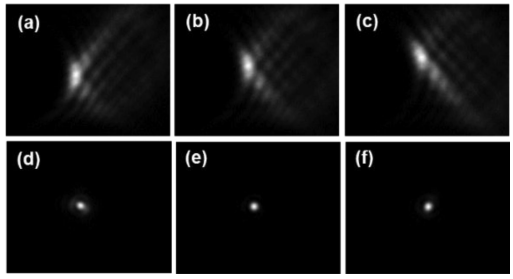

Fig. 6. Focusing process before (a–c) and after (d–f) aberration correction, (b) and (e) are the focus patterns on the focal plane, while (a, d) and (c, f) are the patterns before and after the focal plane with the same defocus of 8 mm.

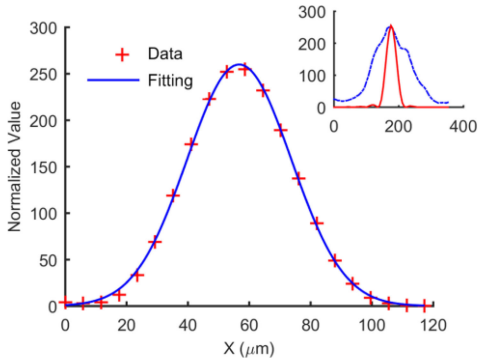

Fig. 7. Intensity profile along the horizontal line across the center of the focus in Fig. 6(e), along with a Gaussian fitting (only interesting data are presented.). Inset: intensity profiles along the vertical lines across the center of the focuses before (blue dashed curve) and after (red solid curve) aberration correction. The intensity has been normalized to 255. Two pictures have the same x and y labels.

was small. That means after correction, the phase distribution is nearly flat. It can be interpreted as direct evidence of aberration correction.

However, although it is hard to observe with eyes, there still exists little fluctuation in the ROI of Fig. 5(b) as its STD is 0.24 instead of 0. So it doubted that whether the 0.24 is good enough and whether the aberration has been truly fully corrected.

As the focus of lens is very sensitive to aberrations, therefore experiments that test the focus pattern of lens before and after aberration correction were performed. We used the SLM to simulate a spherical lens with a focal length of 1000 mm. If there was no aberration, the incident wavefront on CMOS should be an ideal spherical wave with a focal length of 250 mm, as there was a relay system of ratio 1/2 between the SLM and CMOS.

The patterns before and after aberration correction are given in Fig. 6(a–c) and Fig. 6(d–f), respectively. The middle column in Fig. 6 corresponds to the focal plane, while the left and right columns correspond to planes with defocus distances –8 mm and 8 mm, respectively. The intensity profiles along the vertical lines across the centre of Fig. 6(b) (blue dashed curve) and Fig. 6(e) (red solid curve) are given in the inset of Fig. 7.

In Fig. 6(b), because of the large amount of aberrations, the focus was significantly degraded and its width was large. However, as can be seen in Fig. 6(e), after appropriate correction wavefront was applied to the SLM, the light was focused onto a small point again and its width became smaller as presented in the inset of Fig. 7. Moreover, from Fig. 6(a–c), one can see that the focus was shifted laterally during propagation, implying tilt aberration. However, from Fig. 6(d–f) it can be seen that the lateral location did not change anymore. That means the tilt aberration has been corrected.

For quantitative analysis, Fig. 7 also shows the intensity profile at the horizontal line across the centre of the focus in Fig. 6(e), along with Gaussian fitting. From Fig. 7 we can see that after

aberration correction, the full width at half-maximum (FWHM) of focus was 41.0 μm. On the CMOS plane, the radius of ROI was 1.7 mm. The reconstruction distance was 246 mm and the wavelength of laser light was 473 nm. Thus, if there was no aberration, theoretically the diffraction limit is 41.8 μm. The measured FWHM was close to the theoretical value. Therefore, our method has indeed fully corrected the aberration and recovered a diffraction-limited focus.

We should point out that in the defocused patterns in Fig. 6(d) and (f), small amount of aberrations still existed. It can be improved with smaller threshold value or data with higher signal to noise ratio. However, here after three iterations, the aberration has already been corrected to an acceptable level. From the experimental results, we can see that aberrations have been corrected with the correction wavefront, proving the correctness of modal wavefront.

4. Conclusion

In conclusion, we have proposed a simple but effective method to find the modal estimation of wavefront in optical systems. After measuring the wavefront, it can be analysed automatically with 1D standard polynomial fitting. From the modal estimation, the amounts of aberration are acquired. Moreover, the optimal correction wavefront can be calculated accordingly. It is determined automatically and algorithmically. As this method is based on simple 1D polynomial fitting instead of professional ZPF, it is more users friendly. Meanwhile, as confirmed by the experimental results, this method is effective and does not present any compromise because of its simplicity. This method provides users with another option for aberration interpretation. Besides of flexibility, theoretically it does not have strict request on the shape of aperture as the ZPF and it is effective even if some data are missing.

Acknowledgment

The authors would like to thank Sheng Xiao (Boston University) for his useful discussion.

References

[1] T. Cizmar, M. Mazilu, and K. Dholakia, "In situ wavefront correction and its application to micromanipulation," (in English), *Nature Photon.*, vol. 4, no. 6, pp. 388–394, Jun. 2010.
[2] M. Born and E. Wolf, *Principles of Optics*, 7th ed. Cambridge, U.K.: Cambridge Univ., 2005.
[3] R. K. Tyson, *Principles of Adaptive Optics*. San Diego, CA, USA: Academic, 1991.
[4] S. Grilli, P. Ferraro, S. D. Nicola, A. Finizio, G. Pierattini, and R. Meucci, "Whole optical wavefields reconstruction by digital holography," *Opt. Exp.*, vol. 9, no. 6, pp. 294–302, Sep. 10, 2001.
[5] W. J. Bates, "A wavefront shearing interferometer," in *Proc. Phys. Soc.*, 1947, vol. 59, no. 6, Art. no. 940.
[6] F. Roddier, "Curvature sensing and compensation: A new concept in adaptive optics," *Appl. Opt.*, vol. 27, no. 7, pp. 1223–1225, Apr. 1, 1988.
[7] R. Shack and B. Platt, "Production and use of a lenticular Hartmann screen," *J. Opt. Soc. Amer.*, vol. 61, pp. 656–661, 1971.
[8] A. Jesacher, A. Schwaighofer, S. Fürhapter, C. Maurer, S. Bernet, and M. Ritsch-Marte, "Wavefront correction of spatial light modulators using an optical vortex image," *Opt. Exp.*, vol. 15, no. 9, pp. 5801–5808, Apr. 30, 2007.
[9] R. W. Gerchberg, "A practical algorithm for the determination of phase from image and diffraction plane pictures," *Optik*, vol. 35, pp. 237–250, 1972.
[10] C. Maurer, A. Jesacher, S. Bernet, and M. Ritsch-Marte, "What spatial light modulators can do for optical microscopy," *Laser Photon. Rev.*, vol. 5, no. 1, pp. 81–101, 2011.
[11] D. C. Dayton, S. L. Browne, S. P. Sandven, J. D. Gonglewski, and A. V. Kudryashov, "Theory and laboratory demonstrations on the use of a nematic liquid-crystal phase modulator for controlled turbulence generation and adaptive optics," *Appl. Opt.*, vol. 37, no. 24, pp. 5579–5589, Aug. 20, 1998.
[12] R. Dou and M. K. Giles, "Closed-loop adaptive-optics system with a liquid-crystal television as a phase retarder," *Opt. Lett.*, vol. 20, no. 14, pp. 1583–1585, Jul. 15, 1995.
[13] E. J. Fernández and P. Artal, "Membrane deformable mirror for adaptive optics: Performance limits in visual optics," *Opt. Exp.*, vol. 11, no. 9, pp. 1056–1069, May 5, 2003.
[14] W. Jiang, N. Ling, X. Rao, and F. Shi, "Fitting capability of deformable mirror," *SPIE*, 1991, vol. 1542, pp. 130–137, 1991.
[15] R. Hudgin, "Wave-front compensation error due to finite corrector-element size," *J. Opt. Soc. Amer.*, vol. 67, no. 3, pp. 393–395, Mar. 1, 1977.
[16] D. Débarre, E. J. Botcherby, T. Watanabe, S. Srinivas, M. J. Booth, and T. Wilson, "Image-based adaptive optics for two-photon microscopy," *Opt. Lett.*, vol. 34, no. 16, pp. 2495–2497, Aug. 15, 2009.

[17] R. K. Tyson, *Principles of Adaptive Optics*, 3rd ed. Boca Raton, FL USA:CRC Press, 2011.
[18] R. Cubalchini, "Modal wave-front estimation from phase derivative measurements," *J. Opt. Soc. Amer.*, vol. 69, no. 7, pp. 972–977, Jul. 7, 1979.
[19] F. Dai, F. Tang, X. Wang, O. Sasaki, and P. Feng, "Modal wavefront reconstruction based on Zernike polynomials for lateral shearing interferometry: Comparisons of existing algorithms," *Appl. Opt.*, vol. 51, no. 21, pp. 5028–5037, Jul. 20, 2012.
[20] J. Y. Wang and D. E. Silva, "Wave-front interpretation with Zernike polynomials," *Appl. Opt.*, vol. 19, no. 9, pp. 1510–1518, May 1, 1980.
[21] N. Ji, D. E. Milkie, and E. Betzig, "Adaptive optics via pupil segmentation for high-resolution imaging in biological tissues," *Nature Methods*, vol. 7, no. 2, pp. 141–147, 2010.
[22] N. Ji, "Adaptive optical fluorescence microscopy," *Nature Methods*, vol. 14, no. 4, pp. 374–380, Apr. 2017.
[23] I. M. Vellekoop and A. P. Mosk, "Focusing coherent light through opaque strongly scattering media," *Opt. Lett.*, vol. 32, no. 16, pp. 2309–2311, Aug. 15, 2007.
[24] I. M. Vellekoop and A. P. Mosk, "Phase control algorithms for focusing light through turbid media," (in English), *Opt. Commun.*, vol. 281, no. 11, pp. 3071–3080, Jun. 1, 2008.
[25] I. M. Vellekoop, A. Lagendijk, and A. P. Mosk, "Exploiting disorder for perfect focusing," (in English), *Nature Photon.*, vol. 4, no. 5, pp. 320–322, May 2010.
[26] I. M. Vellekoop, "Feedback-based wavefront shaping," *Opt. Exp.*, vol. 23, no. 9, pp. 12189–12206, May 4, 2015.
[27] P. Pozzi *et al.*, "High speed wavefront sensorless aberration correction in digital micromirror based confocal microscopy," *Opt. Exp.*, vol. 25, no. 2, pp. 949–959, Jan. 23, 2017.
[28] G. M. Dai, *Wavefront Optics for Vision Correction*. Bellingham, WA, USA: SPIE, 2008.
[29] I. Yamaguchi, T. Matsumura, and J. Kato, "Phase-shifting color digital holography," (in English), *Opt. Lett.*, vol. 27, no. 13, pp. 1108–1110, Jul. 2002.
[30] D. C Ghiglia and M. D Pritt, *Two-Dimensional Phase Unwrapping: Theory, Algorithms, and Software*. Hoboken, NJ USA: Wiley, 1998.
[31] A. Augusto and C. Roman, "Estimation and compensation of aberrations in spatial light modulators," *J. Phys. Conf. Series*, vol. 274, no. 1, 2011, Art. no. 012060.
[32] K. D. Wulff *et al.*, "Aberration correction in holographic optical tweezers," (in English), *Opt. Exp.*, vol. 14, no. 9, pp. 4169–4174, May 1, 2006.